Progress In Electromagnetics Research M, Vol. 62, 131–141, 2017

A Horizon Ring Nulling Shorted Annular Patch Antenna with Shunted Stubs

Ian T. McMichael*, Erik T. Lundberg, Drayton L. Hanna, and Frank S. Kolak

Abstract—A dual-band shorted annular ring patch antenna with interference rejection at the horizon is presented for GPS timing applications. It is shown that the dimensions of the annular ring can be optimized to make a null in the RHCP pattern at low elevation near the horizon for all azimuth angles. This null attenuates interfering signals originating from ground based sources. The antenna achieves circular polarization utilizing radial shunted stubs. The effect of the stubs on the resonance is analytically derived and verified through simulations. A novel feed configuration that incorporates a coplanar waveguide transition improves the impedance match for both L1 and L2 GPS frequency bands compared to previous designs that present compromises between the feed impedance of the two bands. Additionally, since the shunted stubs reduce the number of required electronic components compared to other antennas with similar horizon nulling capability, the cost is reduced. A prototype antenna operating at GPS L1 and L2 bands has been fabricated and validated through measurements.

1. INTRODUCTION

Global positioning system (GPS) antennas are frequently used to receive accurate timing information from GPS satellite constellations. These antennas are critical for a variety of applications where synchronization and accurate timing is required. GPS timing antennas at fixed site infrastructures are susceptible to inference. This interference can come from out-of-band and multipath signals as well as intentional interference from ground based commercial GPS jammers [1].

Accurate GPS systems rely on receiving signals from multiple satellites simultaneously. For GPS timing, the required number of satellites is fewer than that required for accurate positioning. Depending on receiver design and algorithm implementation, either 2 or 3 satellites are required for reliable timing with satellite fault detection and exclusion [2]. It has been determined that a GPS timing antenna with a half power beamwidth (HPBW) of 60° will have access to 3 satellites 95% of the time. The proposed antenna creates a null at the horizon for interference rejection at the expense of a narrower HPBW compared to a conventional GPS patch antenna.Conventional GPS patch antennas used for positioning have a HPBW in the range of 90° to 120° depending on the patch size and ground plane size.Conventional GPS antennas also have a gain of at least -7.5 dBic at the horizon to receive sufficient power from low elevation satellites [3]. In contrast, it is acceptable for the horizon null of the proposed antenna to block energy at the horizon since the timing application does not require low elevation satellites.

Other types of GPS antennas have been developed to mitigate interference, such as controlled reception pattern antennas (CRPA). A CRPA steers a null in the direction of the interference using

Received 25 August 2017, Accepted 11 October 2017, Scheduled 15 November 2017
* Corresponding author: Ian T. McMichael (imcmichael@mitre.org).
The authors are with the MITRE Corporation, Bedford, MA 01730, USA. Direct-contract funded by Office of the Secretary of Defense, contract W56KGU-14-0010; does not constitute an express or implied endorsement of the results or conclusions by OSD or U.S. Dept. of Defense. Approved for Public Release; Distribution Unlimited. Case Number 17-1165.

active circuitry [3]. While CRPAs can achieve exceptional nulling in a specific direction, they can be costly and physically large due to the multiple antenna elements necessary for null steering. CRPAs are typically expensive due to the active electronics and are limited to nulling a finite number of interferers. Fixed reception pattern antennas (FRPA) can also be designed to mitigate interference from a known direction. One FRPA example is the horizon ring nulling (HRN) antenna that was previously developed, which achieved a measured RHCP null depth (i.e., zenith-to-horizon gain ratio) of approximately 45 dB around all azimuth [4]. The HRN is composed of a shorted annular ring patch combined with a circular patch with amplitude and phase weighting to create a fixed null at the horizon. While the HRN's nulling performance is exceptional with respect to its RHCP horizon nulling capability, the cost is relatively high compared to the antenna proposed in this paper. The higher cost of the HRN is due to the required electronics. Additionally, the exceptional null of the HRN degrades significantly when installed in typical environments with other scattering objects nearby.

In this paper, a horizon nulling shorted annular patch (SAP) antenna with shunted stubs is presented for the application of GPS timing. The salient features of this antenna include a deep null in the right-hand circular polarized (RHCP) gain pattern at the horizon and shunted stubs, which create circular polarization with as few as one feed port. The horizon null spans a full ring around azimuth to greatly reduce ground based interference. This low cost printed circuit board (PCB) architecture with shunted stubs reduces the number of electronic components necessary to support circular polarization and horizon nulling. This method reduces the manufacturing cost compared to antennas with similar horizon nulling performance.

Section 2 of this paper describes the shorted annular patch antenna with shunted stubs and horizon nulling capability. Section 3 describes a prototype antenna and shows simulated and measured results, followed by conclusions in Section 4.

2. SHORTED ANNULAR PATCH WITH SHUNTED STUBS

2.1. Shorted Annular Patch with Horizon Null

The shorted annular patch (SAP) antenna is a well-known design that has been studied extensively for its reduced surface wave property. It has been shown that when the outer radius of the ring is a critical value, surface waves are not excited [5]. It has also been shown that the antenna pattern of the SAP antenna can be shaped by the selection of the ring's outer radius. This is accomplished while maintaining the desired resonant frequency that is associated with the ratio of the outer radius to the inner radius [6]. The outer radius is typically designed to suppress surface waves, which limits the range of gain pattern shaping. It will be shown that if the surface wave constraint is relaxed, the location of a deep null in the gain pattern can be controlled and placed precisely at the horizon. Surface waves are acceptable for the proposed antenna since typical installation geometries isolate it from other antennas. It should be noted that the proposed antenna was not designed to minimize multipath signals, which are typically manifested in left-hand circular polarized (LHCP) energy. While the LHCP gain is significantly lower at the horizon as compared to zenith RHCP gain, no effort was made to minimize

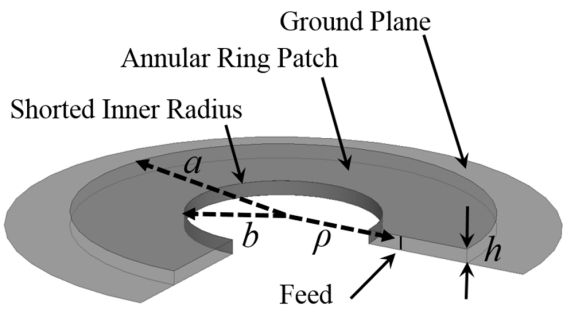

Figure 1. A conventional shorted annular ring patch antenna is shown with a cross section removed to display detail of the shorted inner radius, annular ring patch, ground plane and feed.

LHCP and RHCP horizon gain simultaneously. A conventional shorted annular patch is made of a planar ring over a thin grounded dielectric substrate. The ring's inner radius is shorted to ground as shown in Figure 1, which is an example of single frequency SAP for simplicity. The short is realized in the current PCB antenna design with closely spaced (approximately $\lambda/50$) plated-through holes, or vias. In the proposed design, two SAP antennas are stacked to operate at both L1 (1.575 GHz) and L2 (1.227 GHz) GPS frequencies. The bottom L2 patch acts as the ground plane for the upper L1 patch, as shown in Figure 2. The stacked dual band configuration is more compact than having separate L1 and L2 antennas side by side on a shared ground plane.

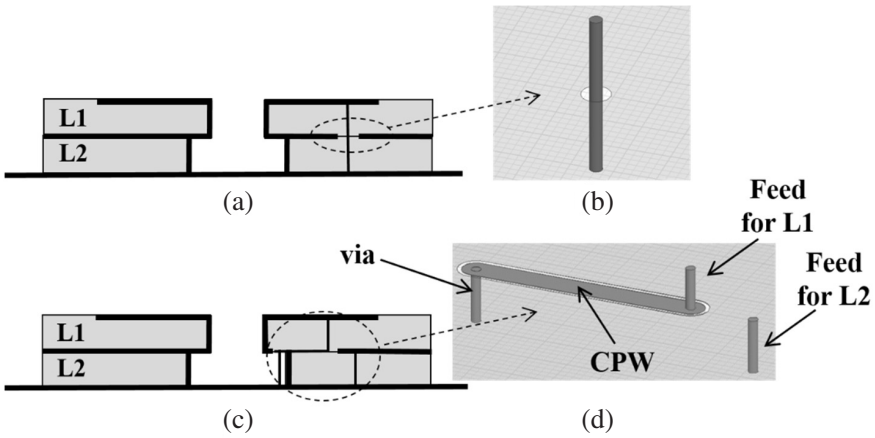

Figure 2. (a) Cross section view of a stacked SAP antenna with a conventional single feed pin exciting both L1 and L2 frequencies. (b) Isometric detail view of the single feed pin. (c) Cross section view of a stacked SAP antenna with a CPW transition between the L1 and L2 pins for improved impedance matching. (d) isometric detail view of the CPW transition between the L1 and L2 feed pins.

2.2. Dual Band Feed Configuration

The SAP antenna impedance varies from 0 Ω at the shorted inner radius to 200–300 Ω at the outer radius [7]. The position of the feed, shown as ρ in Figure 1, can be chosen to optimally match to 50 Ω. This optimal feed position is different for the L1 and L2 layers. Previous designs used a single feed position that compromised between the L1 and L2 impedances. This configuration is shown in Figures 2(a) and (b) [4]. When using a single feed for two frequencies, the two frequencies must be spectrally separated using a diplexer before filtering and amplification. In order to impedance match each feed independently and reduce cost by eliminating the need for a diplexer, a novel SAP antenna feed configuration was developed. In this design, the lower L2 layer is exited with a feed pin extending from the ground plane to the L2 annular patch. The upper L1 layer is fed independently with a coplanar waveguide (CPW) section that is embedded within the L2 patch. The 50 Ω CPW section extends from inside the shorted annular patch to the L1 excitation radius as shown in Figures 2(c) and (d). In this manner, the L1 and L2 feeds can be placed independently to optimize impedance matching for both frequency bands. Additionally, the L1 and L2 signals can be routed directly into independent filtering and amplification stages without the need for a diplexer.

2.3. Shunted Stubs for Circular Polarization

Circular polarization is typically enforced by exciting the shorted annular patch with multiple (typically 4) feed pins separated by 90 degrees and fed in quadrature [3]. In this paper, a method is presented that requires only one feed position using shunted stubs to achieve circular polarization. This method reduces the number of circuit components for phasing and combining signals, thereby reducing manufacturing cost and RF loss. The design method is derived from the standard practice of introducing perturbation segments to produce degenerate orthogonal modes using a single feed [8, 9]. In this case, the novel

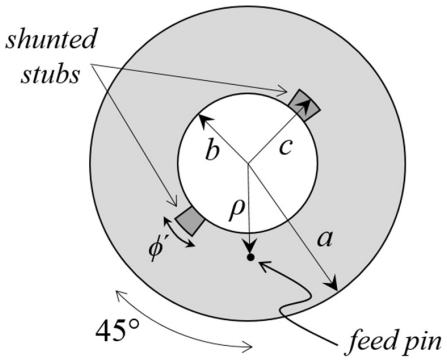

Figure 3. Top view of a shorted annular patch antenna with shunted stubs to create circular polarization with a single feed.

perturbation segment is a shunted stub extending radially from the shorted inner radius of the SAP out to a prescribed distance, illustrated in Figure 3. Ideally, the stub consists of a continuous metal boundary, but is realized here using closely spaced vias allowing for low-cost PCB manufacturing. Two stubs are located 180° apart from each other in the annular ring. Additionally, the stubs are positioned either 45° and 225° in the clockwise direction from the feed pin as viewed from the top for RHCP, or 45° and 225° in the counter-clockwise direction for LHCP. For the application of GPS timing, RHCP is required, so the stubs are clocked accordingly.

The resonant frequency of the orthogonal modes created by the shunted stubs are derived as follows. The SAP resonant frequency is given by [10]

$$f_{mn} = \frac{k_{mn} c_0}{2\pi a_{\mathit{eff}} \sqrt{\varepsilon_r}}, \tag{1}$$

where c_0 is the free space wave velocity, ε_r the substrate relative permittivity, and k_{mn} are the roots of the characteristic equation

$$J'_m(k_{mn}) N_m\left(k_{mn}\frac{b_{\mathit{eff}}}{a_{\mathit{eff}}}\right) - J_m\left(k_{mn}\frac{b_{\mathit{eff}}}{a_{\mathit{eff}}}\right) N'_m(k_{mn}) = 0. \tag{2}$$

In Eq. (2), J_m and N_m are the mth order Bessel functions of the first and second kinds, respectively, and the prime denotes the first derivative [10]. The characteristic Equation (2) is derived from the boundary conditions of the SAP antenna, as discussed in detail in [11]. The dimension a_{eff} is a correction value for the patch outer radius that accounts for fringing fields, which is given in [10] as

$$a_{\mathit{eff}} = a + \kappa h. \tag{3}$$

The constant κ in Eq. (3) is given as 0.75 in [10] for a SAP that has a substrate extending beyond the patch to the edge of the ground plane. However, for the prototype antenna presented here, the substrate only extends to the edge of the patch, and we get a better agreement for the predicted resonance with a value of $\kappa = 0.5$. As introduced in [12], the dimension b_{eff} in Eq. (2) is equivalent to b when the thin stubs are $\pm 90°$ from the feed pin. When the shunted stubs are aligned with the feed pin, b_{eff} is the effective inner radius of the patch, which is given by

$$b_{\mathit{eff}} = b + \Delta s. \tag{4}$$

The perturbation segment, Δs, effectively extends the inner radius internally. It is assumed that the SAP height is electrically small and the fields in the vertical direction are constant, so the height of the stub, h, does not affect the resonance.

The perturbation segment is derived as

$$\Delta s = (c - b) \int_0^{\Phi'/2} \cos\varphi d\varphi, \tag{5}$$

where

$$\Phi' = \varphi' + \frac{2\,(c-b)}{c}. \tag{6}$$

The angular width of the stub, ϕ' shown in Figure 3, has units of radians. Equation (5) defines an effective change in the SAP inner radius when the feed is aligned with the stub as shown in Figure 4(a). Since the vertical electric fields, E_z, for the TM_{11} mode of the SAP antenna are proportional to $\cos\phi$ [10], where $\phi = 0°$ is the location of the feed pin, the cumulative contribution of the stub falls off with the cosine of its angular width. The second term on the right-hand side of Eq. (6) was derived empirically and accounts for the fringing fields around the stub. These fringing fields make the effective stub width larger than its physical width.

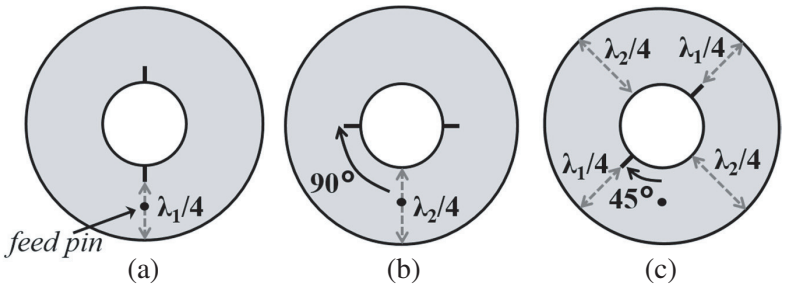

Figure 4. (a) SAP with shunted stubs aligned with the feed. (b) SAP with shunted stubs offset 90° from the feed. (c) SAP with shunted stubs offset 45° from the feed.

Since E_z for the TM_{11} mode of the SAP antenna is proportional to $\cos\phi$, the field strength is negligible at $\phi = 90°$. When the stub is sufficiently thin, it will not affect the resonance if located at $\phi = 90°$, as shown in Figure 4(b). In this manner, the effective inner radius creates a different resonance when the feed pin is aligned with one of the stubs compared to when the feed pin is offset by 90°.

When the shunted stubs are located at $\phi = \pm 45°$ and $\pm 225°$, as shown in Figure 4(c), two orthogonal modes are excited. The resonance of one of the modes is defined by the inner radius, b, while the other resonant mode is defined by the effective inner radius due to the shunted stubs, b_{eff}, shown in Eq. (4). These two orthogonal modes are in quadrature and have equal amplitude at an intermediate frequency between the two resonances, which satisfies the condition for circular polarization.

In order to validate the resonance predicted by Equations (1)–(6), a shorted annular patch antenna was simulated in the configuration shown in Figure 4(a) with HFSS, a full-wave finite element solver. The angular width of the shunted stub, ϕ', was varied from 0° to 180° while all other dimensions remained constant. For this analysis, the stubs were modeled as a solid metal vertical stub protruding radially from the shorted inner patch radius.The simulated antenna, shown in Figure 5, has a patch outer radius of $a = 2.422$ inches and an inner radius of $b = 1.276$ inches. The substrate has a height of $h = 0.125$ inches and a substrate relative dielectric constant of 2.2. The ground plane has a radius of 3.5 inches and the feed pin is $\rho = 1.7$ inches from the center of the antenna. Figure 6 shows that the simulated resonant frequencies are in good agreement with the predicted resonance of Equations (1)–(6).

When the shunted stubs are offset from the feed by 45°, as shown in Figure 4(c), circular polarization is achieved. To demonstrate that circular polarization is achieved at the intermediate frequency between the two orthogonal modes, the antenna from Figure 5 was simulated with a 1.6° wide shunted stub offset by 0°, 45°, and 90° from the feed. The other stub was positioned 180° from the first stub for each angular offset case. Figure 7 shows the reflection coefficient for the GPS L1 antenna with these three different stub offsets and similarly Figure 8 shows the reflection coefficients at GPS L2. It can be seen that the resonant frequency is highest when the stubs are aligned with the feed and the resonant frequency is lowest when the stubs are offset by 90°.

It is demonstrated that when the stubs are offset by 45°, energy is dissipated in both modes. That is, the reflection coefficient has a broader response. This is not to imply that circular polarization is achieved over this entire band. In contrast to the reflection coefficient, the axial ratio is only optimized over a relatively narrow frequency band. Figure 9 shows the GPS L1 axial ratio for the 45° stub offset

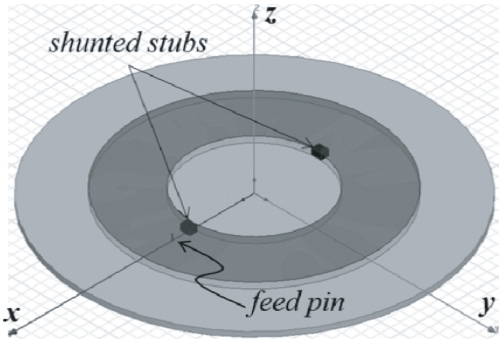

Figure 5. HFSS model of a shorted annular patch with shunted stubs aligned with the feed. The angular width of the stubs was varied from 0°–90° and the resonance was recorded for comparison to the resonance predicted by Equations (1)–(6).

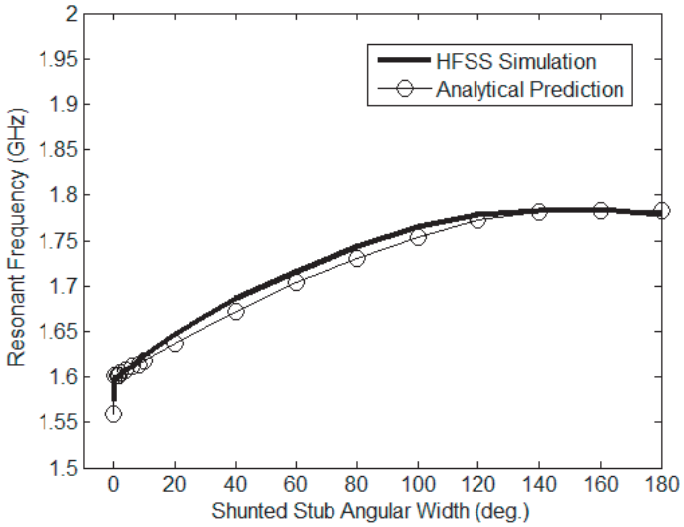

Figure 6. Simulated and analytically derived resonance vs. shunted stub angular width for the antenna shown in Figure 5.

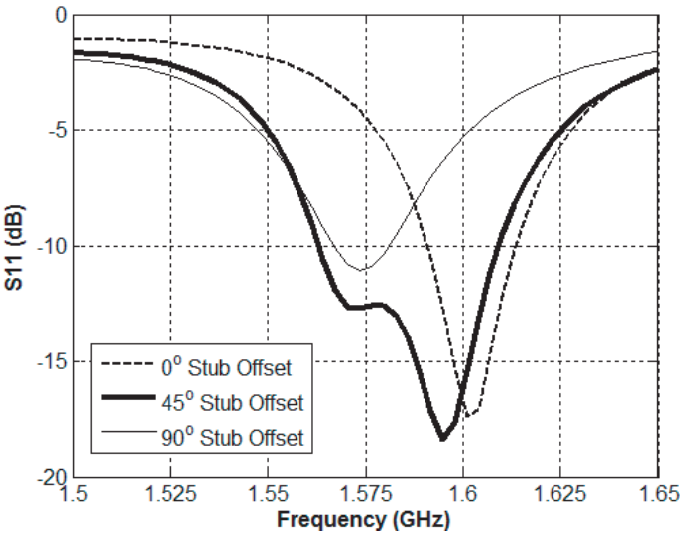

Figure 7. Simulated reflection coefficient for an L1 shorted annular patch with shunted stubs offset 0°, 45°, and 90° from the feed.

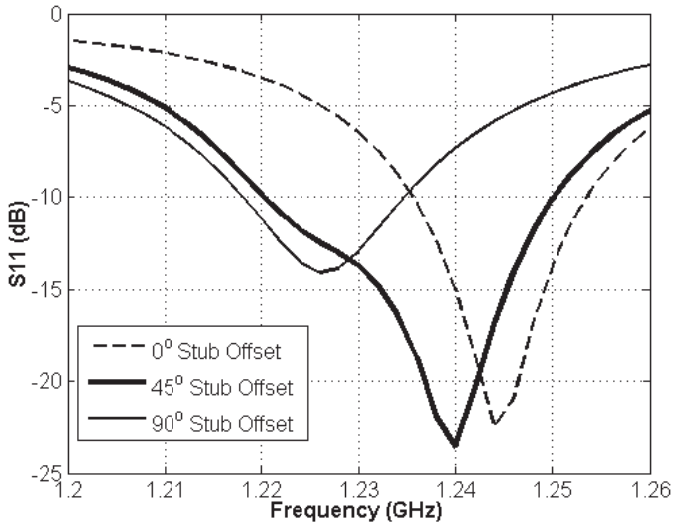

Figure 8. Simulated reflection coefficient for an L2 shorted annular patch with shunted stubs offset 0°, 45°, and 90° from the feed.

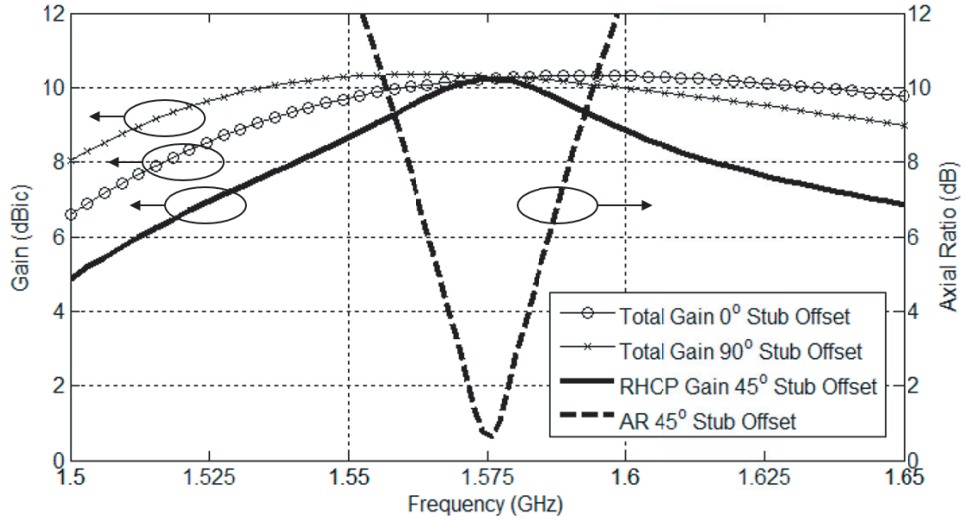

Figure 9. Simulated L1 gain for a shorted annular patch with shunted stubs offset 0°, 45°, and 90° from the feed compared to the axial ratio for the 45° stub offset.

as well as the gain of the antenna with the three different stub offsets. Figure 10 shows the response at GPS L2. The plots show that the axial ratio is optimized when the orthogonal mode amplitudes are equal and falls off rapidly away from the crossover frequency. The simulated axial ratio is 0.6 dB at GPS L1 and is 2.0 dB at GPS L2. These values are sufficient for GPS timing applications.

3. PROTOTYPE ANTENNA

A dual band shorted annular patch with shunted stubs was prototyped and measured. Both L1 and L2 stacked antenna layers, as shown in Figure 11, use the same type of substrate: 0.10-inch thick Rogers 5870, which has a dielectric constant of 2.33 and a loss tangent of 0.001. The upper L1 patch has an outer radius of 2.442 inches, an inner radius of 1.367 inches, and a feed radius of 1.730 inches. The shunted stubs on the L1layer extend 0.135 inches radially from the annular patch inner radius and are 0.024 inches wide, which is the diameter of the vias used to make the stubs. This stub width corresponds

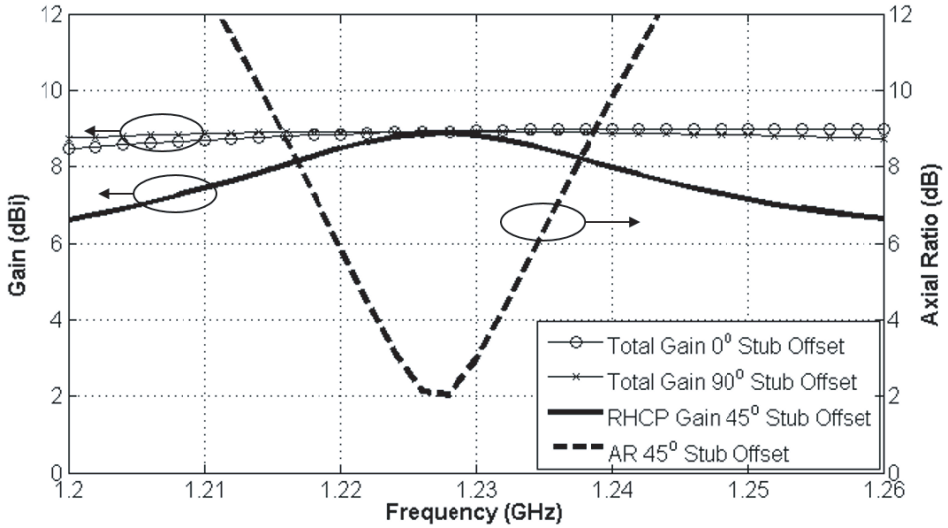

Figure 10. Simulated L2 gain for a shorted annular patch with shunted stubs offset 0°, 45°, and 90° from the feed compared to the axial ratio for the 45° stub offset.

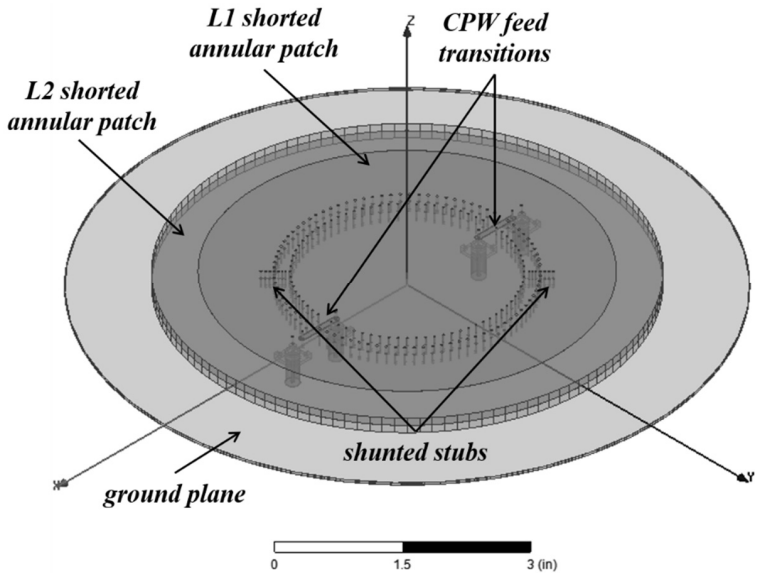

Figure 11. HFSS model of the dual band shorted annular patch antenna with shunted stubs.

to an angular width of 0.9°. The lower L2 annular patch has an outer radius of 2.986 inches, an inner radius of 1.557 inches, and a feed radius of 1.890 inches. The shunted stubs on the L2 layer extend 0.150 inches radially from the annular patch inner radius and are 0.024 inches wide, corresponding to an angular width of 0.8°. The bottom ground plane has a radius of 4.0 inches. A CPW section is used to feed the two antenna layers at different radii for independent impedance matching as explained in Section 2.

While the method of achieving circular polarization discussed in Section 2.3 requires only a single feed, simulations showed a more symmetric gain pattern with two feeds positioned 180° apart. Near perfect symmetry and axial ratio can be achieved without any shunted stubs by implementing four feed ports fed in quadrature. However, this method requires a more complex combiner network. Therefore, a trade-off between performance and complexity/cost resulted in the decision to design the antenna with shunted stubs and two feed ports. This improves the pattern symmetry at the expense of requiring

a 180° combiner network. The resulting antenna is shown in Figure 11. In Figure 11, each layer is semi-transparent to show detail. It should be noted that the shorted inner radius of the patches and the shunted stubs are composed of closely spaced vias to facilitate PCB fabrication. Figure 12 shows the manufactured prototype antenna.

The simulated and measured reflection coefficients for GPS L1 and L2 are shown in Figure 13. The GPS frequency bandwidth is shaded in the plots. It can be seen that the measured antenna resonance is slightly lower than the simulated resonance for both L1 and L2. This may be caused by small differences between the simulated and manufactured substrate dielectric constant or other manufacturing tolerances. This indicates that the antenna performance is sensitive to material and manufacturing tolerances and might benefit by increasing the antenna bandwidth with a thicker substrate.

The antenna gain patterns, which were measured in an anechoic chamber, are shown in Figure 14 along with the simulated gain patterns at the L1 and L2 center frequencies. It is shown that the horizon null in the measured patterns is not as deep or symmetric as the simulated patterns. As with the reflection coefficient, this points to the sensitivity of this antenna to manufacturing tolerances.Additionally, it can be seen that the measured zenith gain is less than the simulated zenith gain. It is theorized that the lower RHCP gain in measurements is due to degraded axial ratio, material losses, and loss in the 180° combiner network.

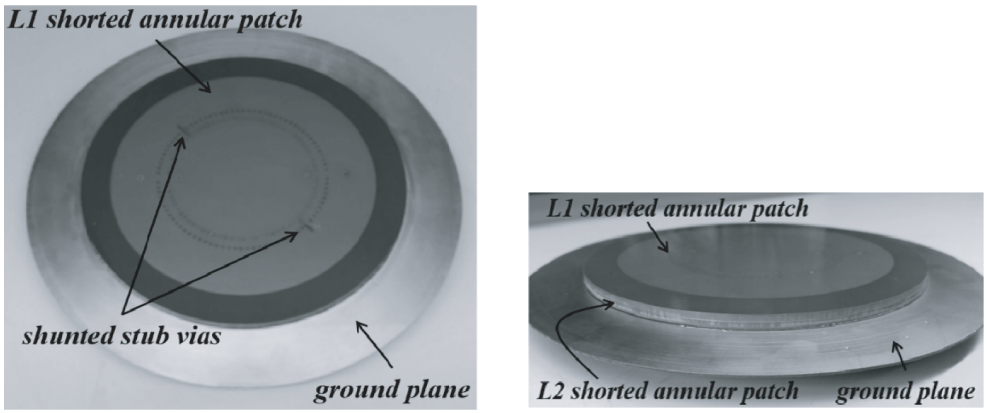

(a) (b)

Figure 12. (a) Top view and (b) side view of the dual band shorted annular patch with shunted stubs manufactured with standard PCB processes.

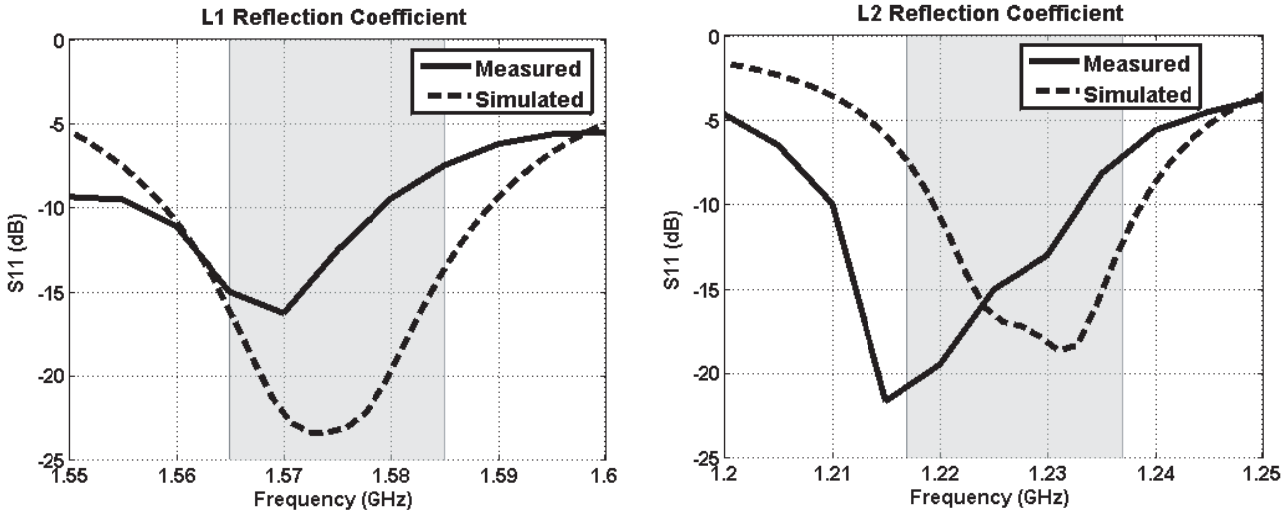

(a) (b)

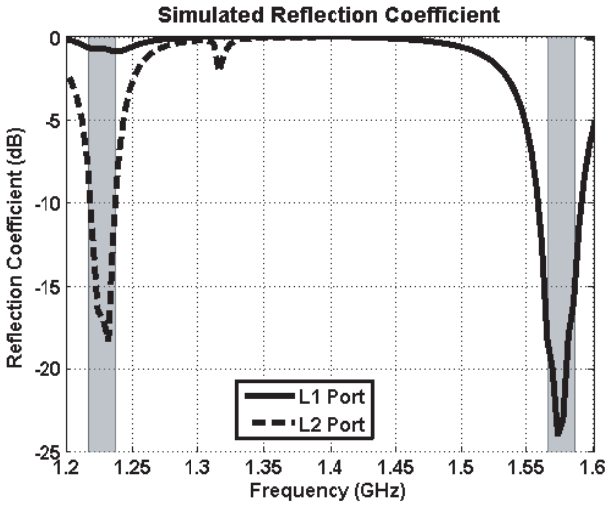

(c)

Figure 13. (a) L1 measured and simulated reflection coefficient. (b) L2 measured and simulated reflection coefficient and (c) simulated L1 and L2 reflection coefficient between the two bands. The shaded regions indicate the frequency bandwidth of each GPS band.

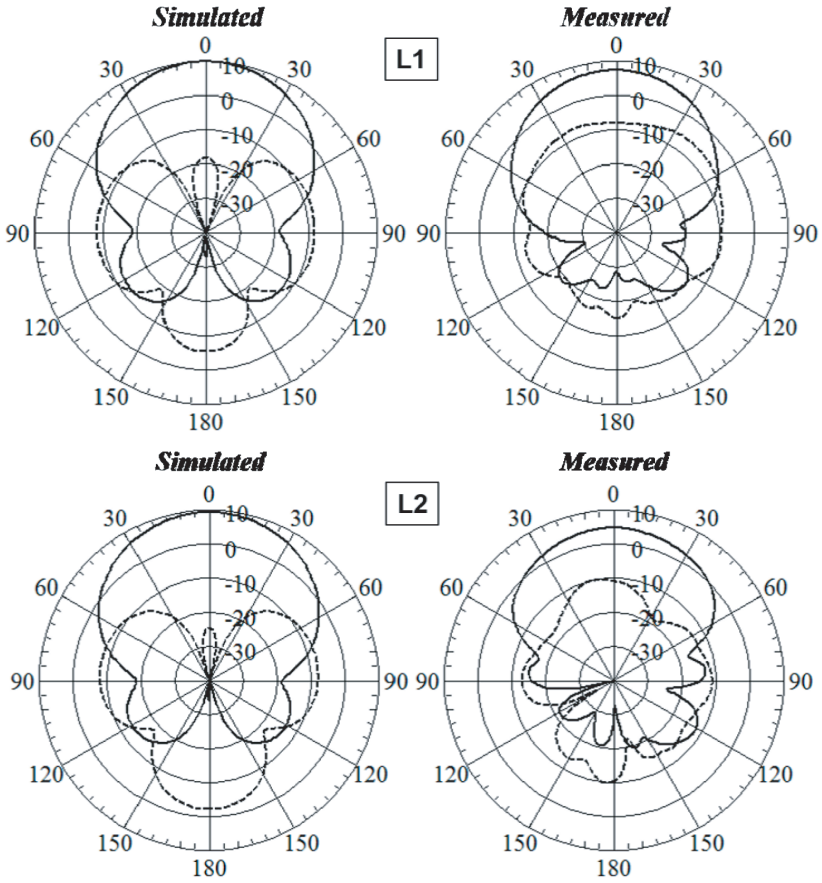

Figure 14. Simulated and measured gain patterns for the L1 (1.575 GHz) and L2 (1.227 GHz) center frequencies. Solid lines indicate RHCP gain and dashed lines indicate LHCP gain.

4. CONCLUSIONS

A dual-band horizon ring nulling shorted annular patch with shunted stubs was presented for the application of GPS timing. The RHCP gain pattern has a deep null at the horizon to suppress interference from ground based sources. The zenith beamwidth is broad enough to receive signals from the required number of satellites. A novel feature of this antenna is the shunted stubs, which are used to create circular polarization with as few as one feed port. Secondly, a novel CPW feed transition was presented for independently impedance matching the L1 and L2 frequency bands. The antenna was designed to be manufactured using standard PCB processes to reduce cost.

Measured results were similar to simulations, but it was evident that variations in substrate material properties and manufacturing tolerances can affect the performance of the antenna. The overall design architecture is versatile enough that it may also find applications for nulling LHCP ground based interference. This would be accomplished by clocking the stubs for an LHCP zenith beam, which would place a null in the LHCP gain pattern at the horizon.

REFERENCES

1. Kaplan, E., *Understanding GPS Principles and Applications*, Artech House, 1996.
2. Geier, G., T. King, H. Kennedy, R. Thomas, and B. McNamara, "Prediction of the time accuracy and integrity of GPS timing," *Proc. IEEE International Frequency Control Symposium*, 226–274, San Francisco, USA, 1995.
3. Rao, B. R., W. Kunysz, R. Fante, and K. McDonald, *GPS/GNSS Antenna*, Artech House, 2012.
4. Rao, B. R. and E. Rosario, "Spatial null steering microstrip antenna array," U.S. Patent 6,597,316, Jul. 22, 2003.
5. Jackson, D., A. Bhattaacharyya, R. Smith, S. Buchheit, and S. Long, "Microstrip patch designs that do not excite surface waves," *IEEE Trans. Antennas Propagat.*, Vol. 41, 1026–1037, Aug. 1993.
6. Boccia, L., G. Amendola, and G. Di Massa, "A dual frequency microstrip patch antenna for high-precision GPS applications," *IEEE Ant. Wireless Propagat. Letters*, Vol. 3, 157–160, 2004.
7. Massa, G. and G. Mazzarella, "Shorted annular patch antenna," *Microwave and Optical Technology Letters*, Vol. 8, No. 4, 222–226, Mar. 1995.
8. Haneishi, M., T. Nambara, and S. Yoshida, "Study on ellipticity properties of single-feed-type circularly polarised microstrip antennas," *Electronics Letters*, Vol. 18, No. 5, Mar. 1982.
9. Young, M., *The Techincal Writers Handbook*, University Science, Mill Valley, CA, 1989.
10. Gonzalez-Posadas, V., D. Segovia-Vargas, E. Rajo-Iglesias, J. Luis Vazquez-Roy, and C. Martin-Pascual, "Approximate analysis of short circuited ring patch antenna working at TM_{01} mode," *IEEE Trans. Antennas Propagat.*, Vol. 54, No. 6, Jun. 2006.
11. Lin, Y. and L. Shafai, "Characteristics of concentrically shorted circular patch microstrip antennas," *IEE Proceedings*, Vol. 137, Pt. H, No. 1, 18–24, Feb. 1990.
12. McMichael, I., E. Lundberg, D. Hanna, and F. Kolak, "Horizon ring nulling shorted annular patch GNSS antenna with shunted stubs," *2016 IEEE International Symposium on Antennas and Propagation (APSURSI)*, 1101–1102, Fajardo, Puerto Rico, 2016.